Nanoscale

PAPER

View Article Online
View Journal | View Issue

Cite this: *Nanoscale*, 2022, **14**, 11972

Alkyl group-decorated g-C_3N_4 for enhanced gas-phase CO_2 photoreduction†

Chao Yang,[a] Yanting Hou,[a] Guoqiang Luo,[b] Jiaguo Yu[a] and Shaowen Cao *[a]

Received 10th May 2022,
Accepted 27th July 2022

DOI: 10.1039/d2nr02551e

rsc.li/nanoscale

With excellent physical/chemical stability and feasible synthesis, g-C_3N_4 has attracted much attention in the field of photocatalysis. However, its weak photoactivity limits its practical applications. Herein, by easily planting hydrophobic alkyl groups onto g-C_3N_4, the hydrophilicity of g-C_3N_4 can be well regulated and its specific surface area be enlarged simultaneously. Such a modification ensures enhanced CO_2 capture and increased active sites. In addition, the introduction of alkyl groups endows g-C_3N_4 with abundant charge density and efficient separation of photoinduced excitons. All these advantages synergistically contribute to the enhanced photocatalytic CO_2 reduction performance over the optimized catalyst (DCN90), and the total CO_2 conversion is 7.4-fold that of pristine g-C_3N_4 (CN).

Introduction

Photocatalytic CO_2 reduction into high value-added chemical fuels is able to simultaneously mitigate the increasingly severe energy crisis and environmental problems, which is considered as one of the photochemical reactions with the most potential.[1–7] To apply photocatalytic CO_2 reduction technology in practice, the main research aim is to seek the proper photocatalyst. In recent decades, polymeric g-C_3N_4 has received great attention as a promising photocatalyst because of its excellent physical and chemical stability, easy synthesis methods, low cost, abundant resources, and visible-light response, *etc.*[8–10] Nevertheless, due to the fast recombination of photogenerated charge carriers, insufficient active sites, and weak CO_2 adsorption, the CO_2 reduction performance of g-C_3N_4 is commonly unsatisfactory.[11–14]

To promote the photocatalytic activity of g-C_3N_4, plentiful strategies have been developed so far. For example, crafting heterojunctions or loading cocatalysts is an effective approach to boost the separation of photogenerated charge carriers.[15–17] To provide more active sites, designing unique nanostructures is obviously crucial, which also favors the process of mass transfer including CO_2 capture and the desorption of reduction products.[18] Recently, upon introducing electron donor or acceptor units into the framework of g-C_3N_4, the obtained donor–acceptor-based g-C_3N_4 has demonstrated enhanced light-harvesting capacity and efficient separation of charges due to the strong electron push–pull effect.[19,20]

Although these methods play a positive role in improving photocatalytic CO_2 reduction performance, there still exists an imperative scientific issue that is usually neglected. As is known, during gas-phase CO_2 photoreduction, the simultaneous adsorption of H_2O and CO_2 molecules on the surface of the photocatalyst jointly determines the reaction rate.[21,22] Specifically, the oxidation of H_2O molecules to provide protons is considered as a rate-determining step. A beneficial H_2O adsorption process can accelerate the oxidation of H_2O for the fast supplementation of protons. However, excessive H_2O adsorption will occupy the CO_2 adsorption sites, resulting in the weakening of the CO_2 hydrogenation process.[23,24] Therefore, a good adsorption balance between CO_2 and H_2O molecules is very significant, which is rarely investigated now.

Herein, we achieve the facile regulation of the hydrophilicity of g-C_3N_4 by planting hydrophobic alkyl groups. It is found that the decline in the hydrophilicity of g-C_3N_4 trades off against the enhanced CO_2 adsorption. In addition, the specific surface area of g-C_3N_4 is also enlarged, thus providing more active sites. Most importantly, the introduction of alkyl groups increases the electron density of g-C_3N_4 and promotes the dissociation of photogenerated charge carriers. These enhancements synergistically improve the photocatalytic CO_2 reduction performance, and the total CO_2 conversion over the optimal sample (DCN90) is 7.4-fold that of pristine g-C_3N_4. This research offers a straightforward and effective strategy for the design of highly efficient g-C_3N_4-based photocatalysts for energy conversion.

---

[a] *State Key Laboratory of Advanced Technology for Materials Synthesis and Processing, Wuhan University of Technology, Wuhan 430070, China. E-mail: swcao@whut.edu.cn*

[b] *Chaozhou Branch of Chemistry and Chemical Engineering Guangdong Laboratory, Chaozhou 521000, China*

† Electronic supplementary information (ESI) available. See DOI: **https://doi.org/10.1039/d2nr02551e**

Results and discussion

Fig. 1a shows the synthesis route of alkyl group-functionalized g-C_3N_4. Under illumination, a series of radical reactions occur on the surface of g-C_3N_4 (CN), which can trigger the occurrence of additional reactions between CN and 1-decene (Fig. S1†),[25] thus successfully obtaining hydrophobic alkyl group-grafted g-C_3N_4 (DCNT, T is the irradiation time, T = 30, 60, 90, and 120 min). The X-ray diffraction (XRD) patterns and Fourier transform infrared spectra (FTIR) were recorded to investigate the chemical structures of the samples (Fig. S2 and S3†). Compared with CN, the XRD peak position and the FTIR spectra of DCNT show no obvious change, indicating that the chemical structure of CN is well retained after planting alkyl groups.[26] Notably, the DCNT samples possess wider XRD peaks (~27°) than those of CN, which might result from the insertion of alkyl groups into the interlayer of CN.[27]

To further analyze the chemical structures of the samples, X-ray photoelectron spectra (XPS) were recorded. Fig. S4a† shows that both CN and DCN90 mainly consist of the C, N, and O elements and the O content in the DCN90 sample is lower than that of CN. As shown in Fig. S4b,† the high-resolution N 1s spectra of CN and DCN90 can be fitted into three peaks, respectively, attributed to sp^2-hybridized nitrogen (C–N=C), tri-coordinated nitrogen (N–C_3), and the terminal amino groups (–NH_x).[28–30] From Fig. 1b, the high-resolution C 1s spectrum of CN consists of three sub-peaks, indexed to sp^2-hybridized carbon (N–C=N), C–OH from adsorbed H_2O, and adventitious carbon impurities, respectively.[31–33] As for the DCN90 sample, a new peak located at 283.9 eV appears, which is assigned to sp^3-hybridized C–H from the alkyl groups.[34] Meanwhile, the peak assigned to the adsorbed H_2O disappears. These results suggest that the hydrophobic alkyl groups have been successfully grafted onto the surface of CN *via* photoinduced grafting, thus leading to a decrease in H_2O adsorption, which can be further confirmed by the weaker high-resolution O 1s spectrum for DCN90 (Fig. 1c).[35] In addition, the peak positions of N–C=N and C–N=C shift to lower binding energies for DCN90 compared with CN, which is attributed to the increased electron density of g-C_3N_4 after grafting alkyl groups.

The introduction of hydrophobic alkyl groups could exert an imperative effect on the physical and chemical properties of CN. Therefore, the hydrophilicity of the samples was first explored. As shown in Fig. 2a, with prolonged photoinduced grafting time, the water contact angles of the samples gradually increase from 60° (CN) to 83° (DCN90). This result indicates a slightly decreased H_2O adsorption capacity. The field emission scanning electron microscopic (FESEM) images show that CN exhibits a nanosheet-like morphology (Fig. S5a†). After grafting the alkyl groups, the morphology of CN is still retained (Fig. S5b–e†), which can be further confirmed by the transmission electron microscopic (TEM) images (Fig. S6†). Atomic force microscopy (AFM) was applied to measure the thickness of the samples.[36] Fig. 2b provides the AFM image of CN and the corresponding height profile shows a thickness of 61.7 nm (the inset of Fig. 2b). Compared with CN, the DCN90 sample is thinner with a thickness of around 10 nm (Fig. 2c and the inset of Fig. 2c). This can be explained by the insertion of alkyl groups into the interlayer of CN, resulting in the exfoliation of CN, which is consistent with the results of XRD.

In general, the thinner thinness of g-C_3N_4 signifies the larger specific surface area (S_{BET}).[37] To confirm this point, the N_2 adsorption–desorption isotherms of CN and DCN90 were measured. As shown in Fig. 2d, both CN and DCN90 exhibit type-IV isotherms with an H3-type hysteresis loop.[38] The corresponding pore size distribution curves of CN and DCN90 mainly display the mesopores and macropores. Compared with CN, the DCN90 sample possesses a higher N_2

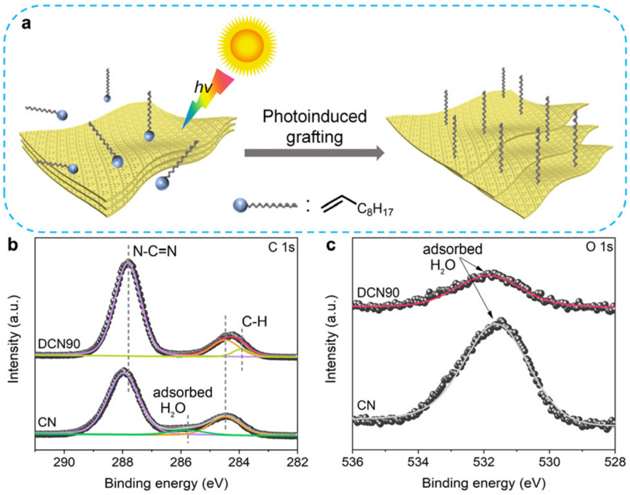

Fig. 1 (a) Synthesis route of alkyl group-functionalized g-C_3N_4 with controlled hydrophilicity. High-resolution XPS (b) C 1s and (c) O 1s spectra of CN and DCN90.

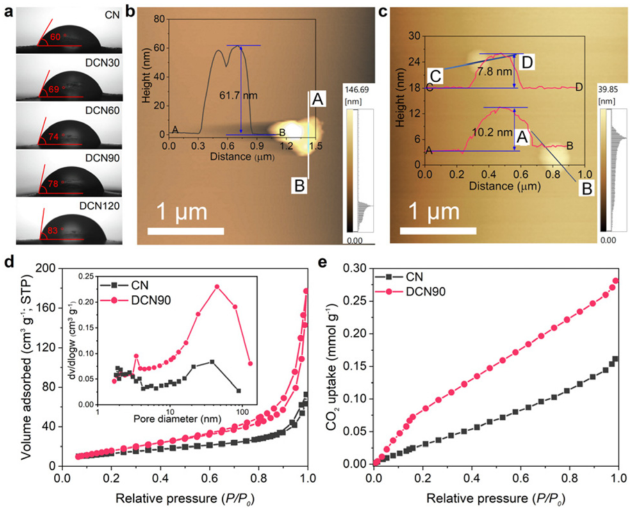

Fig. 2 (a) Water contact angles of the samples. AFM images and the corresponding height profiles (insets) of (b) CN and (c) DCN90. (d) N_2 adsorption–desorption isotherms, the corresponding pore size distribution curves (inset of (d)), and (e) the CO_2 uptake curves of CN and DCN90.

adsorption capacity and pore volume (inset of Fig. 2d), thus showing a larger S_{BET} for DCN90 (66 $m^2 g^{-1}$) than for CN (48 $m^2 g^{-1}$). As is known, the larger S_{BET} favors providing more adsorbed and active sites.[39,40] Accordingly, the CO_2 adsorption performance of CN and DCN90 was further tested. Fig. 2e shows that the CO_2 uptake amount of DCN90 is 0.28 mmol g^{-1} at a relative pressure (P/P_0) of 1, obviously higher than that of CN (0.16 mmol g^{-1}). The slightly decreased hydrophilicity and enhanced CO_2 adsorption might boost the adsorption balance between the H_2O and CO_2 molecules,[21] which is beneficial for the progress of the interfacial CO_2 reduction reaction.

To analyze the electronic structures of the samples, the UV–vis diffuse reflectance spectra (DRS) were first recorded to investigate the light-harvesting ability of the samples. As shown in Fig. 3a, upon grafting the hydrophobic alkyl groups, all the samples show enhanced light absorption in the UV region. However, in the visible region, the light absorption performance of samples shows no obvious change. In addition, the absorption edges of samples even display a slight blue-shift, which can be assigned to the typical quantum confinement effect,[41] resulting from the decreased thickness of the samples by inserting the alkyl groups into the interlayer of g-C_3N_4. The absorption edges of CN and DCN90 are respectively 450 and 439 nm, and the corresponding band gaps (E_g) are 2.75 and 2.82 eV. The Mott–Schottky curves were analysed to determine the conduction band potential (E_{CB}) of the samples (Fig. S7†). The values of E_{CB} for CN and DCN90 are respectively −1.29 and −1.44 V (*vs.* Ag/AgCl, pH = 6.7), which can be transformed to −1.11 and −1.26 V (*vs.* NHE, pH = 7) using the conversion formulae S1 and S2.[42] Based on their E_g, the valence band potential (E_{VB}) of CN and DCN90 is 1.64 and 1.56 V, respectively. Fig. 3b illustrates the band structure of CN and DCN90. The more negative E_{CB} for DCN90 allows for a stronger electron driving force for CO_2 photoreduction.[43]

As is known, the separation of photoinduced charge carriers plays a critical role in a photocatalytic reaction.[44] Consequently, the electron paramagnetic resonance (EPR) spectra were first recorded to investigate the charge density of the CN and DCN90 samples. Both CN and DCN90 exhibit a single Lorentzian line (g = 2.009) signal (Fig. 3c), attributed to the unpaired electrons from the aromatic heptazine ring.[45] Compared with CN, the EPR signal of DCN90 is obviously enhanced. This is due to the introduction of alkyl groups because the alkyl groups act as electron donors for supplying more delocalized electrons.[46] Furthermore, the time-resolved photoluminescence (PL) spectra were recorded to investigate the PL lifetime of the samples (Fig. 3d). According to the tri-exponential decay fit (Table 1), the PL lifetimes of CN and DCN90 are calculated to be 28.2 and 22.1 ns, respectively. The decreased lifetime indicates a faster electron transfer for DCN90 than CN, which could be attributed to the establishment of a built-in electric field between alkyl groups and g-C_3N_4.[47] The steady-state PL spectra show that the PL intensity of DCN90 is obviously weakened compared with CN (Fig. 3e), suggesting the more efficient separation of photogenerated charges for DCN90, which is attributed to the decreased thickness of DCN90 for quick electron transfer from the bulk to the surface.[48–50] In addition, the PL peak of DCN90 shows a blue shift compared with CN, resulting from the quantum confinement effect due to the decreased thickness of DCN90. The photocurrent tests show that DCN90 possesses a stronger photocurrent signal than CN. When the photocurrent signal is steady, DCN90 shows a slower decay of the photocurrent signal compared with CN whether the light source is on or off (Fig. 3f). This result indicates that DCN90 possesses a slower recombination of photogenerated charges than CN. The decreased electrochemical impedance for DCN90 further confirms the improved transfer of photogenerated charges after grafting alkyl groups (Fig. S8†).[51] The more delocalized electrons and efficient separation of charges demonstrate the higher photocatalytic performance.

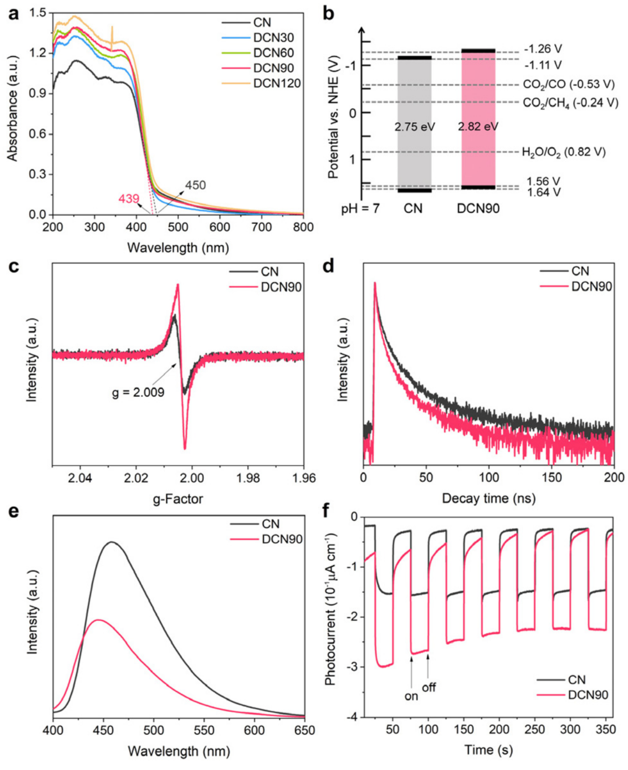

Fig. 3 (a) UV–vis DRS spectra of various samples. (b) Electronic band structure, (c) EPR spectra, (d) time-resolved PL spectra, (e) steady-state PL spectra, and (f) transient photocurrent response of the CN and DCN90 samples.

Table 1 Summary of the photoluminescence decay time (τ) and their pre-exponential factor (B) of the CN and DCN90 samples. The calculation formula of average lifetime is as follows: $\tau_{ave} = (B_1\tau_1^2 + B_2\tau_2^2 + B_3\tau_3^2)/(B_1\tau_1 + B_2\tau_2 + B_3\tau_3)$

	Decay time (ns)			Pre-exponential factor (%)			
Samples	τ_1	τ_2	τ_3	B_1	B_2	B_3	τ_{ave} (ns)
CN	1.59	7.44	35.56	20.87	47.70	31.43	28.2
DCN90	1.08	5.29	27.67	20.41	48.55	31.04	22.1

To evaluate the photocatalytic activity of the samples, CO_2 reduction tests were carried out under full spectrum irradiation without any cocatalyst or sacrificial reagent. Fig. 4a shows that CO is the primary CO_2 reduction product, along with a small amount of CH_4. This is because the reduction of CO_2 into CO follows the two-electron reduction process, which is easier than the eight-electron reduction of CO_2 into CH_4. Unmodified CN shows a very low photocatalytic performance, and the yields of CO and CH_4 are 2.61 and 0.20 μmol h^{-1} g^{-1}, respectively. After grafting hydrophobic alkyl groups onto g-C_3N_4, the photocatalytic activity of samples is greatly enhanced. In particular, DCN90 exhibits an optimal CO_2 reduction performance with yields of 19.77 μmol h^{-1} g^{-1} for CO and 1.09 μmol h^{-1} g^{-1} for CH_4, which are higher than many reported results (Table 2). The total CO_2 conversion of DCN90 is 7.4-fold that of CN.

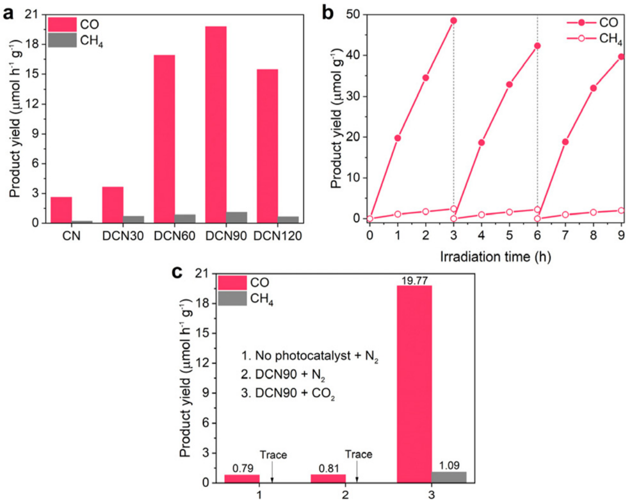

Fig. 4 (a) Photocatalytic CO_2 reduction performance of various samples. (b) Cycle tests and (c) control experiments of CO_2 photoreduction over the DCN90 sample.

In addition, photocatalytic cycle tests were conducted to investigate the stability of DCN90. After three consecutive runs, 81.7% of the total CO_2 conversion performance of DCN90 is still retained with no obvious change in morphology, hydrophilicity, and chemical structure (Fig. 4b and S9–S11†). A certain degree of decreased activity might be caused by the occupation of active sites due to the adsorption of intermediates on the surface of DCN90. Finally, control experiments were carried out to determine the carbon source of the reduction products. From Fig. 4c, without a photocatalyst and under a N_2 atmosphere, a little CO is observed and no CH_4 is detected. Furthermore, with DCN90 irradiated under a N_2 atmosphere, a very similar result is obtained. The small amounts of CO produced might originate from the pollution of the apparatus.[62] However, when DCN90 is irradiated under a CO_2 atmosphere, a rapidly enhanced CO yield is observed, and CH_4 is also detected. These results strongly affirm that CO and CH_4 are produced by CO_2 photoreduction.

Based on the above results of CO_2 photoreduction and the characterization of the physical and photoelectrochemical properties of the samples, a rational photocatalytic mechanism is

Table 2 Comparison of the photocatalytic activity and the reaction conditions with other g-C_3N_4-based photocatalysts for CO_2 reduction (LS, CS, TOR, SR, AOP, TEOA, and MeOH represent the light source, the CO_2 source, the type of reaction, the sacrificial reagent, the amount of photocatalyst, triethanolamine, and methanol, respectively)

Materials	LS	CS	TOR	SR	AOP (mg)	Product yield (μmol h^{-1} g^{-1})	Ref.
DCN90	300 W Xe lamp (full spectrum)	CO_2 gas	Gas–solid	—	50	CO: 19.77 CH_4: 1.09	This work
g-CN-0.01Dbc	300 W Xe lamp	CO_2 gas	Liquid–solid	—	20	CO: 2.4	19
g-C_3N_4/7Ag/m-CeO_2	8 W UV lamp	CO_2 gas	Liquid–solid	TEOA	100	CO: 1.39 CH_4: 0.74	52
$OCCN_{0.25}$	4 W UV lamp (254 nm, 40 μW cm^{-2})	CO_2 gas	Liquid–solid	—	20	CO: 8.74	53
CMN	300 W Xe lamp	CO_2 gas	Gas–solid	—	30	CO: 18.8 CH_4: 1.8	54
10TC	300 W Xe lamp ($\lambda \geq 420$ nm)	$NaHCO_3 + H_2SO_4$	Gas–solid	—	20	CO: 5.19 CH_4: 0.044	16
CFC-0.2	350–780 nm	CO_2 gas	Gas–solid	—	50	CO: 8.182 CH_4: 0.0805	55
2Au-CN	300 W Xe lamp (full spectrum)	CO_2 gas	Gas–solid	—	50	CO: 6.585 CH_4: 1.55	56
3% Ni/NiO/g-C_3N_4	300 W Xe lamp (full spectrum)	CO_2 gas	Gas–solid	—	50	CO: 13.955 CH_4: 2.08	57
Ni_5-CN	300 W Xe lamp ($\lambda \geq 420$ nm)	CO_2 gas	Gas–solid	—	25	CO: 8.6 CH_4: 0.5	58
CABB@C_3N_4-82%	AM1.5G (150 mW cm^{-2})	CO_2 gas	Liquid–solid	MeOH	15	CO: <0.75 CH_4: <1.35	59
5BSCN	300 W Xe lamp (full spectrum)	$NaHCO_3 + H_2SO_4$	Gas–solid	—	50	CO: 8.2	15
BiCN-0.6	AM1.5G	CO_2 gas	Liquid–solid	—	50	CO: 3.78 CH_4: 1.65	60
CZTS-CN	400 W Xe lamp ($\lambda \geq 420$ nm)	CO_2 gas	Gas–solid	—	100	CO: 2.402 CH_4: 0.752	61

proposed. First, under irradiation, the electrons in VB are excited and jump into CB. As for the hydrophobic alkyl group-decorated DCN90, a more negative E_{CB} allows for a stronger electron reduction ability. Furthermore, the electron-rich alkyl groups can increase the charge density of g-C_3N_4 and boost the separation of photogenerated charge carriers. In addition, due to the insertion effect of the hydrophobic alkyl groups, g-C_3N_4 becomes thinner, which enlarges the specific surface area to provide more active sites. Meanwhile, the hydrophilicity of g-C_3N_4 is also regulated to optimize the simultaneous adsorption of H_2O and CO_2 molecules. All these factors synergistically endow DCN90 with a more favorable photoelectronic nature, thus leading to greatly enhanced photocatalytic activity compared with pristine g-C_3N_4.

Conclusions

In summary, hydrophobic alkyl group-decorated g-C_3N_4 is prepared by an easy photoinduced grafting method. The optimal photocatalyst (DCN90) demonstrates excellent photocatalytic CO_2 reduction activity. The yields of CO and CH_4 reach 19.77 and 1.09 μmol h^{-1} g^{-1}, respectively, and the total CO_2 conversion is 7.4-fold that of pristine g-C_3N_4. The promotion of CO_2 photoreduction performance is mainly attributed to the grafting of hydrophobic alkyl groups. On the one hand, alkyl groups regulate the band structure, increase the electron density, and boost the separation of photoinduced charge carriers of g-C_3N_4. On the other hand, alkyl groups are inserted into the interlayer of g-C_3N_4, enlarging the specific surface area to provide more active sites and optimizing the adsorption of H_2O and CO_2 molecules. All these factors synergistically endow hydrophobic alkyl group-modified g-C_3N_4 with enhanced photocatalytic activity. This work offers a straightforward yet effective strategy to design highly efficient g-C_3N_4-based photocatalysts for photocatalytic energy conversion.

Author contributions

Chao Yang: conceptualization, experiments and data processing, formal analysis, and writing – original draft. Yanting Hou: experiments and formal analysis. Guoqiang Luo: resource and writing – review & editing. Jiaguo Yu: resource and writing – review & editing. Shaowen Cao: formal analysis, resource, writing – review & editing and supervision.

Conflicts of interest

There are no conflicts to declare.

Acknowledgements

This work was financially supported by the Key-Area Research and Development Program of Guangdong Province (2021B0707050001), the National Natural Science Foundation of China (51922081, 51961135303, and 51932007), and the Self-Innovation Research Funding Project of Hanjiang Laboratory (HJL202202A001).

References

1 Y. S. Zhou, Z. T. Wang, L. Huang, S. Zaman, K. Lei, T. Yue, Z. A. Li, B. You and B. Y. Xia, Engineering 2D photocatalysts toward carbon dioxide reduction, *Adv. Energy Mater.*, 2021, **11**, 2003159.

2 M. Sayed, F. Y. Xu, P. Y. Kuang, J. X. Low, S. Y. Wang, L. Y. Zhang and J. G. Yu, Sustained CO_2-photoreduction activity and high selectivity over Mn, C-codoped ZnO core-triple shell hollow spheres, *Nat. Commun.*, 2021, **12**, 4936.

3 M. Sayed, J. G. Yu, G. Liu and M. Jaroniec, Non-noble plasmonic metal-based photocatalysts, *Chem. Rev.*, 2022, **122**, 10484–10537.

4 X. G. Fei, H. Y. Tan, B. Cheng, B. C. Zhu and L. Y. Zhang, 2D/2D black phosphorus/g-C_3N_4 S-scheme heterojunction photocatalysts for CO_2 reduction investigated using DFT calculations, *Acta Phys.-Chim. Sin.*, 2021, **37**, 2010027.

5 S. Wageh, A. A. Al-Ghamdi and L. J. Liu, S-scheme heterojunction photocatalyst for CO_2 photoreduction, *Acta Phys.-Chim. Sin.*, 2021, **37**, 2010024.

6 X. Y. Jiang, J. D. Huang, Z. H. Bi, W. J. Ni, G. Gurzadyan, Y. A. Zhu and Z. Y. Zhang, Plasmonic active "hot spots"-confined photocatalytic CO_2 reduction with high selectivity for CH_4 production, *Adv. Mater.*, 2022, **34**, 2109330.

7 N. Lu, M. Y. Zhang, X. D. Jing, P. Zhang, Y. A. Zhu and Z. Y. Zhang, Electrospun semiconductor–based nano-heterostructures for photocatalytic energy conversion and environmental remediation: Opportunities and challenges, *Energy Environ. Mater.*, 2022, DOI: **10.1002/eem2.12338**.

8 Z. F. Chen, S. C. Lu, Q. L. Wu, F. He, N. Q. Zhao, C. N. He and C. S. Shi, Salt-assisted synthesis of 3D open porous g-C_3N_4 decorated with cyano groups for photocatalytic hydrogen evolution, *Nanoscale*, 2018, **10**, 3008–3013.

9 C. L. Zhu, T. Wei, Y. Wei, L. Wang, M. Lu, Y. P. Yuan, L. S. Yin and L. Huang, Unravelling intramolecular charge transfer in donor–acceptor structured g-C_3N_4 for superior photocatalytic hydrogen evolution, *J. Mater. Chem. A*, 2021, **9**, 1207–1212.

10 X. Y. Jiang, Z. Y. Zhang, M. H. Sun, W. Z. Liu, J. D. Huang and H. Y. Xu, Self-assembly of highly-dispersed phosphotungstic acid clusters onto graphitic carbon nitride nanosheets as fascinating molecular-scale Z-scheme heterojunctions for photocatalytic solar-to-fuels conversion, *Appl. Catal., B*, 2021, **281**, 119473.

11 X. Zhao, Y. Y. Fan, W. S. Zhang, X. J. Zhang, D. X. Han, L. Niu and A. Ivaska, Nanoengineering construction of Cu_2O nanowire arrays encapsulated with g-C_3N_4 as 3D spatial reticulation all-solid-state direct Z-scheme photocatalysts for photocatalytic reduction of carbon dioxide, *ACS Catal.*, 2020, **10**, 6367–6376.

12 P. F. Xia, B. C. Zhu, J. G. Yu, S. W. Cao and M. Jaroniec, Ultra-thin nanosheet assemblies of graphitic carbon nitride for enhanced photocatalytic CO_2 reduction, *J. Mater. Chem. A*, 2017, **5**, 3230–3238.

13 Y. Xia, Z. H. Tian, T. Heil, A. Y. Meng, B. Cheng, S. W. Cao, J. G. Yu and M. Antonietti, Highly selective CO_2 capture and its direct photochemical conversion on ordered 2D/1D heterojunctions, *Joule*, 2019, **3**, 2792–2805.

14 Q. L. Xu, Z. H. Xia, J. M. Zhang, Z. Y. Wei, Q. Guo, H. L. Jin, H. Tang, S. Z. Li, X. C. Pan, Z. Su and S. Wang, Recent advances in solar-driven CO_2 reduction over g–C_3N_4-based photocatalysts, *Carbon Energy*, 2022, DOI: 10.1002/cey2.205.

15 Y. H. Huang, K. Wang, T. Guo, J. Li, X. Y. Wu and G. K. Zhang, Construction of 2D/2D Bi_2Se_3/g-C_3N_4 nanocomposite with high interfacial charge separation and photo-heat conversion efficiency for selective photocatalytic CO_2 reduction, *Appl. Catal., B*, 2020, **277**, 119232.

16 C. Yang, Q. Y. Tan, Q. Li, J. Zhou, J. J. Fan, B. Li, J. Sun and K. L. Lv, 2D/2D Ti_3C_2 MXene/g-C_3N_4 nanosheets heterojunction for high efficient CO_2 reduction photocatalyst: Dual effects of urea, *Appl. Catal., B*, 2020, **268**, 118738.

17 D. P. Dong, C. X. Yan, J. D. Huang, N. Lu, P. Y. Wu, J. Wang and Z. Y. Zhang, An electron-donating strategy to guide the construction of MOF photocatalysts toward co-catalyst-free highly efficient photocatalytic H_2 evolution, *J. Mater. Chem. A*, 2019, **7**, 24180–24185.

18 J. Wang, S. W. Cao and J. G. Yu, Nanocages of polymeric carbon nitride from low-temperature supramolecular preorganization for photocatalytic CO_2 reduction, *Sol. RRL*, 2020, **4**, 1900469.

19 X. H. Song, X. Y. Zhang, M. Wang, X. Li, Z. Zhu, P. W. Huo and Y. S. Yan, Fabricating intramolecular donor–acceptor system via covalent bonding of carbazole to carbon nitride for excellent photocatalytic performance towards CO_2 conversion, *J. Colloid Interface Sci.*, 2021, **594**, 550–560.

20 S. J. Wan, J. S. Xu, S. W. Cao and J. G. Yu, Promoting intramolecular charge transfer of graphitic carbon nitride by donor–acceptor modulation for visible-light photocatalytic H_2 evolution, *Interdiscip. Mater.*, 2022, **1**, 294–308.

21 Y. Xia, K. Xiao, B. Cheng, J. G. Yu, L. Jiang, M. Antonietti and S. W. Cao, Improving artificial photosynthesis over carbon nitride by gas–liquid–solid interface management for full light-induced CO_2 reduction to C_1 and C_2 fuels and O_2, *ChemSusChem*, 2020, **13**, 1730–1734.

22 Q. H. Zhang, Y. Xia and S. W. Cao, "Environmental phosphorylation" boosting photocatalytic CO_2 reduction over polymeric carbon nitride grown on carbon paper at air–liquid–solid joint interfaces, *Chin. J. Catal.*, 2021, **42**, 1667–1676.

23 D. Raciti, M. Mao, J. H. Park and C. Wang, Mass transfer effects in CO_2 reduction on Cu nanowire electrocatalysts, *Catal. Sci. Technol.*, 2018, **8**, 2364–2369.

24 A. Li, Q. Cao, G. Y. Zhou, B. V. K. J. Schmidt, W. J. Zhu, X. T. Yuan, H. L. Huo, J. L. Gong and M. Antonietti, Three-phase photocatalysis for the enhanced selectivity and activity of CO_2 reduction on a hydrophobic surface, *Angew. Chem., Int. Ed.*, 2019, **58**, 14549–14555.

25 B. Kumru, M. Antonietti and B. V. K. J. Schmidt, Enhanced dispersibility of graphitic carbon nitride particles in aqueous and organic media via a one-pot grafting approach, *Langmuir*, 2017, **33**, 9897–9906.

26 C. Yang, S. S. Zhang, Y. Huang, K. L. Lv, S. Fang, X. F. Wu, Q. Li and J. J. Fan, Sharply increasing the visible photoreactivity of g-C_3N_4 by breaking the intralayered hydrogen bonds, *Appl. Surf. Sci.*, 2020, **505**, 144654.

27 F. Yang, D. Z. Liu, Y. X. Li, L. J. Cheng and J. H. Ye, Salt-template-assisted construction of honeycomb-like structured g-C_3N_4 with tunable band structure for enhanced photocatalytic H_2 production, *Appl. Catal., B*, 2019, **240**, 64–71.

28 L.-Z. Qin, Y.-Z. Lin, Y.-C. Dou, Y.-J. Yang, K. Li, T. Li and F.-T. Liu, Toward enhanced photocatalytic activity of graphite carbon nitride through rational design of noble metal-free dual cocatalysts, *Nanoscale*, 2020, **12**, 13829–13837.

29 H. Li, F. Li, J. G. Yu and S. W. Cao, 2D/2D FeNi-LDH/g-C_3N_4 hybrid photocatalyst for enhanced CO_2 photoreduction, *Acta Phys.-Chim. Sin.*, 2020, **37**, 2010073.

30 S. Y. Gao, S. J. Wan, J. G. Yu and S. W. Cao, Donor–acceptor modification of carbon nitride for enhanced photocatalytic hydrogen evolution, *Adv. Sustainable Syst.*, 2022, **6**, 2200130.

31 M.-M. Liu, S.-M. Ying, B.-G. Chen, H.-X. Guo and X.-G. Huang, Ag@g-C_3N_4 nanocomposite: An efficient catalyst inducing the reduction of 4-nitrophenol, *Chin. J. Struct. Chem.*, 2021, **40**, 1372–1378.

32 Q. Li, S. C. Wang, Z. X. Sun, Q. J. Tang, Y. Q. Liu, L. Z. Wang, H. Q. Wang and Z. B. Wu, Enhanced CH_4 selectivity in CO_2 photocatalytic reduction over carbon quantum dots decorated and oxygen doping g-C_3N_4, *Nano Res.*, 2019, **12**, 2749–2759.

33 S. R. Tao, S. J. Wan, Q. Y. Huang, C. M. Li, J. G. Yu and S. W. Cao, Molecular engineering of g-C_3N_4 with dibenzothiophene groups as electron donor for enhanced photocatalytic H_2-production, *Chin. J. Struct. Chem.*, 2022, **41**, 2206048–2206054.

34 O. V. Kuznetsov, A. Cole, M. Pulikkathara and V. N. Khabashesku, Sidewall alkylcarboxylation of carbon nanotubes through reactions of fluoronanotubes with functional free radicals, *Russ. Chem. Bull., Int. Ed.*, 2011, **60**, 2212–2221.

35 F. Dong, S. Guo, H. Q. Wang, X. F. Li and Z. B. Wu, Enhancement of the visible light photocatalytic activity of C-doped TiO_2 nanomaterials prepared by a green synthetic approach, *J. Phys. Chem. C*, 2011, **115**, 13285–13292.

36 P. F. Xia, S. W. Cao, B. C. Zhu, M. J. Liu, M. S. Shi, J. G. Yu and Y. F. Zhang, Designing 0D/2D S-scheme heterojunction over polymeric carbon nitride for visible-light photocatalytic inactivation of bacteria, *Angew. Chem., Int. Ed.*, 2020, **59**, 5218–5225.

37 C. Yang, Y. J. Wang, J. G. Yu and S. W. Cao, Ultrathin 2D/2D graphdiyne/Bi_2WO_6 heterojunction for gas-phase CO_2

photoreduction, *ACS Appl. Energy Mater.*, 2021, **4**, 8734–8738.

38 M. Thommes, K. Kaneko, A. V. Neimark, J. P. Olivier, F. Rodriguez-Reinoso, J. Rouquerol and K. S. W. Sing, Physisorption of gases, with special reference to the evaluation of surface area and pore size distribution (IUPAC Technical Report), *Pure Appl. Chem.*, 2015, **87**, 1051–1069.

39 S. W. Cao, Y. J. Wang, B. C. Zhu, G. C. Xie, J. G. Yu and J. R. Gong, Enhanced photochemical CO_2 reduction in the gas phase by graphdiyne, *J. Mater. Chem. A*, 2020, **8**, 7671–7676.

40 S. Wageh, O. A. Al-Hartomy, M. F. Alotaibi and L.-J. Liu, Ionized cocatalyst to promote CO_2 photoreduction activity over core–triple-shell ZnO hollow spheres, *Rare Met.*, 2022, **41**, 1077–1079.

41 R. Shi, F. L. Liu, Z. Wang, Y. X. Weng and Y. Chen, Black/red phosphorus quantum dots for photocatalytic water splitting: From a type I heterostructure to a Z-scheme system, *Chem. Commun.*, 2019, **55**, 12531–12534.

42 Q. Li, Y. Xia, C. Yang, K. L. Lv, M. Lei and M. Li, Building a direct Z-scheme heterojunction photocatalyst by $ZnIn_2S_4$ nanosheets and TiO_2 hollowspheres for highly-efficient artificial photosynthesis, *Chem. Eng. J.*, 2018, **349**, 287–296.

43 M. Zhang, Y. F. Li, W. Chang, W. Zhu, L. H. Zhang, R. X. Jin and Y. Xing, Negative inductive effect enhances charge transfer driving in sulfonic acid functionalized graphitic carbon nitride with efficient visible-light photocatalytic performance, *Chin. J. Catal.*, 2022, **43**, 526–535.

44 C. Cheng, B. W. He, J. J. Fan, B. Cheng, S. W. Cao and J. G. Yu, An inorganic/organic S-scheme heterojunction H_2-production photocatalyst and its charge transfer mechanism, *Adv. Mater.*, 2021, **33**, 2100317.

45 L. Shi, L. Q. Yang, W. Zhou, Y. Y. Liu, L. S. Yin, X. Hai, H. Song and J. H. Ye, Photoassisted construction of holey defective $g\text{-}C_3N_4$ photocatalysts for efficient visible-light-driven H_2O_2 production, *Small*, 2018, **14**, 1703142.

46 J. Echeverría, Alkyl groups as electron density donors in π-hole bonding, *CrystEngComm*, 2017, **19**, 6289–6296.

47 G. G. Zhang, G. S. Li, Z. A. Lan, L. H. Lin, A. Savateev, T. Heil, S. Zafeiratos, X. C. Wang and M. Antonietti, Optimizing optical absorption, exciton dissociation, and charge transfer of a polymeric carbon nitride with ultrahigh solar hydrogen production activity, *Angew. Chem., Int. Ed.*, 2017, **56**, 13445–13449.

48 W. L. Wang, W. L. Zhao, H. C. Zhang, X. C. Dou and H. F. Shi, 2D/2D step-scheme $\alpha\text{-}Fe_2O_3/Bi_2WO_6$ photocatalyst with efficient charge transfer for enhanced photo-Fenton catalytic activity, *Chin. J. Catal.*, 2021, **42**, 97–106.

49 T. M. Su, Z. D. Hood, M. Naguib, L. Bai, S. Luo, C. M. Rouleau, I. N. Ivanov, H. B. Ji, Z. Z. Qin and Z. L. Wu, 2D/2D heterojunction of $Ti_3C_2/g\text{-}C_3N_4$ nanosheets for enhanced photocatalytic hydrogen evolution, *Nanoscale*, 2019, **11**, 8138–8149.

50 K. Wang, X. Z. Feng, Y. Z. Shangguan, X. Y. Wu and H. Chen, Selective CO_2 photoreduction to CH_4 mediated by dimension-matched 2D/2D $Bi_3NbO_7/g\text{-}C_3N_4$ S-scheme heterojunction, *Chin. J. Catal.*, 2022, **43**, 246–254.

51 L. Cheng, P. Zhang, Q. Y. Wen, J. J. Fan and Q. J. Xiang, Copper and platinum dual-single-atoms supported on crystalline graphitic carbon nitride for enhanced photocatalytic CO_2 reduction, *Chin. J. Catal.*, 2022, **43**, 451–460.

52 H. Q. Wang, J. R. Guan, J. Z. Li, X. Li, C. C. Ma, P. W. Huo and Y. S. Yan, Fabricated $g\text{-}C_3N_4/Ag/m\text{-}CeO_2$ composite photocatalyst for enhanced photoconversion of CO_2, *Appl. Surf. Sci.*, 2020, **506**, 144931.

53 X. H. Song, X. Li, X. Y. Zhang, Y. F. Wu, C. C. Ma, P. W. Huo and Y. S. Yan, Fabricating C and O co-doped carbon nitride with intramolecular donor-acceptor systems for efficient photoreduction of CO_2 to CO, *Appl. Catal., B*, 2020, **268**, 118736.

54 F. Li, D. N. Zhang and Q. J. Xiang, Nanosheet-assembled hierarchical flower-like $g\text{-}C_3N_4$ for enhanced photocatalytic CO_2 reduction activity, *Chem. Commun.*, 2020, **56**, 2443–2446.

55 Z. M. Sun, W. Fang, L. Zhao, H. Chen, X. He, W. X. Li, P. Tian and Z. H. Huang, $g\text{-}C_3N_4$ foam/Cu_2O QDs with excellent CO_2 adsorption and synergistic catalytic effect for photocatalytic CO_2 reduction, *Environ. Int.*, 2019, **130**, 104898.

56 H. L. Li, Y. Gao, Z. Xiong, C. Liao and K. M. Shih, Enhanced selective photocatalytic reduction of CO_2 to CH_4 over plasmonic Au modified $g\text{-}C_3N_4$ photocatalyst under UV–vis light irradiation, *Appl. Surf. Sci.*, 2018, **439**, 552–559.

57 C. Q. Han, R. M. Zhang, Y. H. Ye, L. Wang, Z. Y. Ma, F. Y. Su, H. Q. Xie, Y. Zhou, P. K. Wong and L. Q. Ye, Chainmail co-catalyst of NiO shell-encapsulated Ni for improving photocatalytic CO_2 reduction over $g\text{-}C_3N_4$, *J. Mater. Chem. A*, 2019, **7**, 9726–9735.

58 L. Cheng, H. Yin, C. Cai, J. J. Fan and Q. J. Xiang, Single Ni atoms anchored on porous few-layer $g\text{-}C_3N_4$ for photocatalytic CO_2 reduction: The role of edge confinement, *Small*, 2020, **16**, 2002411.

59 Y. Y. Wang, H. L. Huang, Z. Z. Zhang, C. Wang, Y. Y. Yang, Q. Li and D. S. Xu, Lead-free perovskite $Cs_2AgBiBr_6@g\text{-}C_3N_4$ Z-scheme system for improving CH_4 production in photocatalytic CO_2 reduction, *Appl. Catal., B*, 2021, **282**, 119570.

60 J.-W. Gu, R.-T. Guo, Y.-F. Miao, Y.-Z. Liu, G.-L. Wu, C.-P. Duan and W.-G. Pan, Noble-metal-free $Bi/g\text{-}C_3N_4$ nanohybrids for efficient photocatalytic CO_2 reduction under simulated irradiation, *Energy Fuels*, 2021, **35**, 10102–10112.

61 A. Raza, A. A. Haidry and J. Saddique, *In situ* synthesis of $Cu_2ZnSnS_4/g\text{-}C_3N_4$ heterojunction for superior visible light-driven CO_2 reduction, *J. Phys. Chem. Solids*, 2022, **165**, 110694.

62 K. F. Wang, L. Zhang, Y. Su, D. K. Shao, S. W. Zeng and W. Z. Wang, Photoreduction of carbon dioxide of atmospheric concentration to methane with water over CoAl-layered double hydroxide nanosheets, *J. Mater. Chem. A*, 2018, **6**, 8366–8373.